Structure of kinetic Alfvén waves with small transverse scale length

G. J. Morales and J. E. Maggs
Department of Physics and Astronomy, University of California, Los Angeles, Los Angeles, California 90095

(Received 28 May 1997; accepted 30 July 1997)

This analytical study illustrates the spatial pattern of kinetic Alfvén waves excited by a current-modulating disk whose dimension a, transverse to the confining magnetic field, is comparable to the ion sound gyroradius c_s/Ω_i, where c_s is the sound speed and Ω_i the ion cyclotron frequency. The radial structure of the wave azimuthal magnetic field is found to consist of four regions: a Bessel function behavior for $r<a$, a near null at $r\cong a$, and a driven Airy pattern for $r\gg a$ which merges onto the $1/r$ asymptotic region. The pattern spreads at an angle given by $\tan\theta=(\omega/\Omega_i)(c_s/v_A)/2.6$, where ω is the modulation frequency and v_A is the Alfvén speed. This behavior arises because there is a maximum value at finite $k_\perp$ for the ratio of the perpendicular to parallel group velocity, which differs from the cone spreading [G. J. Morales *et al.*, Phys. Plasmas **1**, 3765 (1994)] associated with inertial Alfvén waves. © *1997 American Institute of Physics.* [S1070-664X(97)00711-8]

I. INTRODUCTION

It is well known that shear Alfvén waves exhibit two extreme limits determined by the ratio of the Alfvén speed v_{A0} to the electron thermal speed $\bar{v}_e$ (or alternatively the electron beta, β_e). For $v_{A0}\gg\bar{v}_e$ the modes are known as ''inertial'' Alfvén waves, while in the opposite regime, $v_{A0}\ll\bar{v}_e$, they are referred to as ''kinetic'' Alfvén waves (or KAW). The significant distinction between the two limits arises in the domain of small spatial scales transverse to the confining magnetic field (i.e., large $k_\perp$). This is a physical situation of considerable interest because at large $k_\perp$ these waves develop significant electric fields parallel to the confining magnetic field so that both modes interact with the plasma electrons, albeit in different regions of velocity space. Presently there is considerable interest in understanding the role that these modes play in the formation of auroral beams[1] and in the generation of fast ions in the auroral ionosphere,[2] where both limits of the shear Alfvén wave are naturally encountered due to the variation of the plasma parameters with altitude.[3] Of course, these modes can also play a role in the transport of energy[4,5] in magnetic confinement devices.

The present study aims to illustrate the spatial pattern associated with a KAW having a transverse scale on the order of the ion sound gyroradius $\rho_s=c_s/\Omega_i$, where $c_s=(T_e/M)^{1/2}$ is the sound speed, Ω_i the ion cyclotron frequency, and T_e the electron temperature. This work complements an earlier investigation[6] of the inertial regime in which the consequences of cone-like propagation characteristics[7,8] have been documented and related to a laboratory experiment.[9] A sharp distinction exists between the intrinsic patterns of the inertial and the kinetic Alfvén waves that should help in identifying them in laboratory and spacecraft measurements.

The qualitative features of the radiation pattern associated with a KAW of small transverse scale can be deduced from the infinite medium dispersion relation

$$k_\parallel=\frac{\omega/v_{A0}}{[1+(k_\perp\rho_s)^2]^{1/2}}, \tag{1}$$

where $k_\parallel$ is the wave number parallel to the confining magnetic field and ω is the excitation frequency. The fundamental quantity that determines the propagation path from an axially localized source containing a $k_\perp$ spectrum is the ratio of the perpendicular group velocity, $v_{g\perp}$, to the parallel group velocity, $v_{g\parallel}$. For the dispersion relation of Eq. (1) this ratio is

$$\tan\theta=\frac{v_{g\perp}}{v_{g\parallel}}=\left(\frac{\omega\rho_s}{v_{A0}}\right)\frac{k_\perp\rho_s}{[1+(k_\perp\rho_s)^2]^{3/2}}, \tag{2}$$

which implies that for small $k_\perp\rho_s$ the propagation angle θ of a KAW is proportional to $k_\perp\rho_s$, but for large $k_\perp\rho_s$ it decreases as $(k_\perp\rho_s)^{-2}$. The important consequence is that there exists a maximum angle of propagation given by

$$\tan\theta_M=\left(\frac{\omega\rho_s}{v_{A0}}\right)\frac{2}{(3)^{3/2}}=\frac{\omega}{\Omega_i}\sqrt{\beta_e}\,\frac{2}{(3)^{3/2}}, \tag{3}$$

corresponding to a wave number $k_\perp\rho_s=(2)^{-1/2}$ and where $\beta_e=(c_s/v_{A0})^2$. Thus the radiation pattern of a KAW emerging from a finite source exhibits a maximum angle of spread given by Eq. (3). At angles of propagation smaller than θ_M two different $k_\perp$ values are found to propagate; one has a small value approximately given by $k_\perp\rho_s\approx(v_{A0}/\omega\rho_s)\tan\theta$, and the large one $k_\perp\rho_s\approx[(\omega\rho_s/v_{A0})/\tan\theta]^{1/2}$. The mixture of two different perpendicular scales at a fixed angle of propagation θ gives rise to unusual patterns that are described in detail later.

Although Eq. (3) predicts a maximum angle of spread, this does not correspond physically and mathematically to a cone-like propagation along characteristics, as is the case for the inertial regime whose infinite medium dispersion relation is

$$k_\parallel=\frac{\omega}{v_{A0}}[1+(k_\perp\delta)^2]^{1/2}, \tag{4}$$

 1070-664X/97/4(11)/4118/8/$10.00

where $\delta = c/\omega_{pe}$ is the electron skin-depth, with c the speed of light and ω_{pe} the electron plasma frequency. The corresponding angle of propagation that determines the pattern of an inertial Alfvén wave of short transverse scale is determined by the analog of Eq. (2)

$$\frac{v_{g\perp}}{v_{g\parallel}} = -\left(\frac{\omega\delta}{v_{A0}}\right)\frac{k_\perp\delta}{[1+(k_\perp\delta)^2]^{1/2}}, \tag{5}$$

in which the minus sign indicates that the inertial wave is, in the transverse direction, a backward wave. From Eq. (5) it is seen that for small $k_\perp\delta$, the inertial mode also exhibits an angle of propagation that increases linearly with $k_\perp$, however, in the limit of large $k_\perp\delta$ the angle of propagation becomes independent of $k_\perp$ and results in propagation along the cone angle θ_c given by

$$\tan\,\theta_c = \left(\frac{\omega}{\Omega_i}\right)\left(\frac{m}{M}\right)^{1/2}, \tag{6}$$

where m and M refer to the electron and ion mass, respectively. This is to be compared to Eq. (3) which in terms of similar quantities becomes

$$\tan\,\theta_M = \left(\frac{\omega}{\Omega_i}\right)\frac{\sqrt{\beta_e}}{(2.6)}. \tag{7}$$

Since the KAW exists for $v_{A0} \ll \overline{v_e}$, i.e., β_e much larger than the mass ratio $\beta_e \gg m/M$, the maximum propagation angle θ_M is larger than the cone angle θ_c.

II. FORMULATION

This study considers the simplest model of localized excitation of a KAW in a magnetized plasma in which the electron response can be considered adiabatic and the ion dynamics is well represented by cold fluid equations. Although there are various methods to couple to a KAW, mathematically the simplest to describe is one incorporating an azimuthally symmetric disk whose dimension a, transverse to the confining magnetic field, is comparable to ρ_s. The role of the idealized disk structure (which in an actual experiment[9] may consist of several grids and supports) is to induce an axial current modulation at frequency ω, which for simplicity is taken to be uniform across the disk.

The useful coordinates in this problem consist of a cylindrical system (r,θ,z) centered on the disk with the axial coordinate z aligned with the confining magnetic field (as in Ref. 6). The physical electric and magnetic fields $(\mathbf{E}',\mathbf{B}')$ consistent with the symmetry of excitation are represented in the form

$$\mathbf{E}' = [E_z(r,z,\omega)\hat{z} + E_r(\hat{r},z,\omega)\hat{r}]e^{-i\omega t} + \text{c.c.}, \tag{8}$$

$$\mathbf{B}' = B_\theta(r,z,\omega)\,\hat{\theta}e^{-i\omega t} + \text{c.c.} \tag{9}$$

In the transverse direction the oscillatory current density in this low-frequency regime $(\omega < \Omega_i)$ is the polarization current proportional to $\partial E_r/\partial t$ carried radially by the cold ions. The azimuthal current is negligible because the azimuthal motion of ions and electrons is due to the $\mathbf{E}\times\mathbf{B}$ drift. The relative azimuthal slippage between electrons and ions becomes significant only in a small frequency band close to Ω_i, as is shown in Ref. 6. The radial current density is given by

$$j_r = -\frac{i\omega}{4\pi}\left(\frac{c}{v_A}\right)^2 E_r, \tag{10}$$

in which a representation similar to Eqs. (8) and (9) is used. In Eq. (10) the quantity v_A denotes the actual phase speed of the wave at frequency ω and $k_\perp = 0$,

$$v_A = v_{Ao}[1-(\omega/\Omega_i)^2]^{1/2}, \tag{11}$$

with $v_{Ao} \equiv c(\Omega_i/\omega_{pi})$ the conventional Alfvén speed, in which ω_{pi} is the ion plasma frequency.

In the parallel direction the oscillatory current density j_z is carried by electrons, which in the appropriate adiabatic limit corresponding to a KAW is determined from

$$\frac{\partial^2}{\partial z^2}\,j_z + \frac{im\omega\nu_e}{T_e}\,j_z = i\,\frac{\omega e^2 n_0}{T_e}\,E_z, \tag{12}$$

where n_0 is the unperturbed plasma density, e the quantum of charge, and an effective collision frequency ν_e is included to obtain a qualitative understanding of the role of dissipation. Of course, a full understanding of collisional effects over a broad range of phase velocities requires a kinetic description, and will be the subject of a separate study.

The system of coupled partial differential equations governing the propagation of the electric field associated with an azimuthally symmetric shear mode is

$$\frac{\partial}{\partial z}\left[\frac{\partial}{\partial r}\,E_z - \frac{\partial}{\partial z}\,E_r\right] = k_A^2 E_r, \tag{13}$$

$$\frac{1}{r}\,\frac{\partial}{\partial r}\left[r\left(\frac{\partial}{\partial z}\,E_r - \frac{\partial}{\partial r}\,E_z\right)\right] = \frac{4\pi i\omega}{c^2}\,j_z, \tag{14}$$

where $k_A = \omega/v_A$, and Eq. (10) has been used.

Equations (12)–(14) are solved using a Laplace transform in the z direction and extracting asymptotic wave solutions for $z>0$. This procedure results in decoupled expressions for the fields in terms of the radial Bessel representation:

$$E_z(r,z) = \int_0^\infty dk\; k\; \tilde{E}_z(k)J_0(kr)e^{ik_\parallel(k)z}, \tag{15}$$

$$E_r(r,z) = \int_0^\infty dk\; k\; \tilde{E}_r(k)J_1(kr)e^{ik_\parallel(k)z}, \tag{16}$$

$$B_\theta(r,z) = \int_0^\infty dk\; k\; \tilde{B}_\theta(k)J_1(kr)e^{ik_\parallel(k)z}, \tag{17}$$

where the parallel wave number $k_\parallel$ depends explicitly on the integration wave number k due to the axial electron response

$$k_\parallel(k) = k_A\left[\frac{1+i(\nu_e/\omega)(k\delta)^2}{1+(k\rho_s)^2}\right]^{1/2}. \tag{18}$$

It should be noted from Eq. (18) that the dissipative effect associated with electron collisions is multiplied by the electron skin-depth δ, and not ρ_s, and furthermore it appears in the same form as in the inertial regime. This dependence

causes the spatial patterns of KAW and inertial Alfvén waves to become quite similar in plasmas having large collisionality.

To determine the Bessel-representation coefficients in Eqs. (15)–(17) the solutions are matched to the axial current injected by the idealized disk modulator, i.e.,

$$j_z(r,z=0^+)=\begin{cases} j_0, & r\leqslant a \\ 0, & r>a, \end{cases} \tag{19}$$

and since

$$j_z(r,z)=\int_0^\infty dk\ k\tilde{j}_z(k)J_0(kr)e^{ik_\parallel(k)z}, \tag{20}$$

this implies that

$$\int_0^\infty dk\ k\tilde{j}_z(k)J_0(kr)=\begin{cases} j_0, & r\leqslant a \\ 0, & r>a, \end{cases} \tag{21}$$

whose solution can be identified[10] as

$$\tilde{j}_z(k)=aj_0\,\frac{J_1(ka)}{k}. \tag{22}$$

Neglecting the displacement current in Ampère's law (as is appropriate in this frequency regime) yields

$$k\tilde{B}_\theta(k)=\frac{4\pi}{c}\,\tilde{j}_z, \tag{23}$$

which results in

$$B_\theta(r,z)=\frac{4\pi j_0 a}{c}\int_0^\infty dk\,\frac{J_1(ka)}{k}\,J_1(kr)e^{ik_\parallel(k)z}. \tag{24}$$

To simplify subsequent discussions it is useful to introduce the scaled quantities

$$b(\rho,\xi)=\frac{acB_\theta}{2I_0}, \tag{25}$$

$$\rho=\frac{r}{a},\quad \xi=k_A z, \tag{26}$$

$$K=ka,\quad \Gamma_\parallel=\frac{\nu_e}{\omega}, \tag{27}$$

$$p=\frac{a\omega_{pe}}{c},\quad s=\frac{a}{\rho_s}, \tag{28}$$

where I_0 is the peak alternating (ac) current flowing from an external generator to the disk exciter.

Equation (24) takes the form

$$b(\rho,\xi)=\int_0^\infty dK\,\frac{J_1(K)}{k}\,J_1(K\rho)\exp\left\{i\xi\left[\frac{1+i\Gamma_\parallel(K/p)^2}{1+(K/s)^2}\right]^{1/2}\right\}, \tag{29}$$

which describes the physical quantity most amenable to direct investigation with small induction-coil detectors, i.e., the scaled azimuthal magnetic field.

III. GENERAL FEATURES

The radial profile of the magnetic field is found by numerical integration of Eq. (29). Before proceeding with this, however, it is enlightening to consider analytic expressions for b in various regimes of ρ and ξ. In the limit of negligible collisions, i.e., $\Gamma_\parallel \ll (p/s)^2=(M/m)\beta_e$, the pattern of a KAW of small transverse scale is determined by a single parameter $s=a/\rho_s$, and is given by

$$b(\rho,\xi)=\int_0^\infty dK\,\frac{J_1(K)}{K}\,J_1(K\rho)\exp\left\{\frac{i\xi}{[1+(K/s)^2]^{1/2}}\right\}. \tag{30}$$

For current modulators having large transverse extent (i.e., $s\to\infty$) the pattern is given by

$$b(\rho,\xi)\to e^{i\xi}\int_0^\infty dK\,\frac{J_1(K)}{K}\,J_1(k\rho), \tag{31}$$

which can be identified[11,12] as

$$b(\rho,\xi)\to e^{i\xi}\begin{cases} \dfrac{\rho}{2}, & 0<\rho<1 \\ \dfrac{1}{2\rho}, & 1<\rho<\infty, \end{cases} \tag{32}$$

and is analogous to the radial pattern associated with a wire carrying a uniform current distribution, as expected from the excitation model, but exhibiting an axial wave number corresponding to an Alfvén wave. In this limit ($s=\infty$) no radial spreading of the Alfvén wave occurs, as in the usual ideal magnetohydrodynamic (MHD) description. The factor of 1/2 in Eq. (32) arises because the exciter launches two waves (propagating to $z=\pm\infty$) for a given value I_o of current injected from the generator.

In the radiation zone $\xi\gg 1$, the KAW radiation pattern exhibits different behavior in four distinct ranges of ρ, which we now examine in detail. For large values of ρ ($\rho\to\infty$, $\xi\gg 1$) the dominant contribution to the integral arises from a region of small values of K, i.e.,

$$b(\rho\to\infty,\xi\gg 1)\to\frac{e^{i\xi}}{2}\int_0^\infty dK\ J_1(K\rho)=\frac{e^{i\xi}}{2\rho}. \tag{33}$$

For intermediate values of ρ, not large enough to be in the extreme asymptotic limit of Eq. (33), there is different behavior for large and small K. As discussed earlier in Sec. I, for propagation angles $\theta<\theta_M$ there are large and small $k_\perp$ contributions to the pattern. It is therefore useful to separately consider the contributions to the integral in Eq. (30) arising from small K and large K. For small K the long wavelength behavior b_L arises from the first term in the Taylor expansion of the phase factor in Eq. (30), i.e., for $(K/s)^2\ll 1$

$$b_L\equiv\frac{e^{i\xi}}{2}\int_0^\infty dK\ J_1(K\rho)e^{-i(\xi K^2/2s^2)}=\frac{e^{i\xi}}{2\rho}\left[1-e^{i(\rho^2 s^2/2\xi)}\right]. \tag{34}$$

The corresponding short wavelength behavior b_s is extracted from Eq. (30) by recognizing that this contribution arises from the large-K region in the integrand, so that

$$J_1(K)\to\sqrt{\frac{2}{\pi K}}\sin\left(K-\frac{\pi}{4}\right), \tag{35}$$

but recognizing that the value of $K\rho$ can be arbitrary, hence

$$b_s\equiv\sqrt{\frac{2}{\pi}}\left(\frac{1}{2i}\right)\int_0^\infty\frac{dK}{K^{3/2}}[e^{i(K-\pi/4)} - e^{-i(K-\pi/4)}]J_1(K\rho)e^{i\xi s/K}. \tag{36}$$

Considering the asymptotic behavior, $\xi\gg 1$, implies that the dominant contribution arises from the positive exponential term (because the stationary phase point lies along the integration path), hence

$$b_s\to\sqrt{\frac{2}{\pi}}\frac{e^{-i\pi/4}}{2i}\int_0^\infty\frac{dK}{K^{3/2}}J_1(K\rho)\exp\left[i\left(K+\frac{\xi s}{K}\right)\right], \tag{37}$$

which can be manipulated[13] to the form

$$b_s=\frac{J_1(\sqrt{\xi s}\rho)}{\sqrt{2\xi s}}\exp\left[i\left(2\sqrt{\xi s}-\frac{\pi}{4}\right)\right]. \tag{38}$$

The short wavelength contribution given by Eq. (38) automatically recovers the behavior of b near the axis, i.e., for $\rho\ll 1$, $\xi\gg 1$,

$$b\to\frac{\rho}{(2)^{3/2}}\exp\left[i\left(2\sqrt{\xi s}-\frac{\pi}{4}\right)\right]. \tag{39}$$

There are two interesting features predicted by Eq. (39). One is that near the axis the parallel wave number of the pattern decreases with increasing axial position according to

$$k_\parallel(\rho\to 0,\xi\gg 1)\to k_A\sqrt{\frac{s}{\xi}}, \tag{40}$$

which is to be compared to the radially asymptotic value predicted by Eq. (33)

$$k_\parallel(\rho\gg 1,\xi\gg 1)\to k_A. \tag{41}$$

The other feature is that the coefficient multiplying the linear increase with radius (at fixed ξ) is independent of ξ and its magnitude is smaller by a factor of $2^{-1/2}$ from that given by Eq. (32) for a large exciter. Physically this implies that for exciters having small transverse scale there is a focusing of the pattern towards the axis of symmetry ($\rho=0$, $\xi\gg 1$) which results in an axially constant current density, albeit reduced in amplitude due to the spreading that occurs in the region $\rho>1$. Note, however, for ρ finite, the compression of the current on-axis is accompanied by short scale radial oscillations described by the $J_1(\sqrt{\xi s}\rho)$ term of Eq. (38).

For intermediate values of ρ, i.e., $1<\rho<\rho_c$, where $\rho_c=\xi\tan\theta_M$ is the critical scaled radius corresponding to the maximum angle of propagation, the approximate behavior of the radiation pattern can be obtained by the superposition of the long and short scale contributions $b\to b_L+b_s$. However, at radial distances close to ρ_c the separation into short and long scales is not correct because a coalescence occurs. The behavior near ρ_c can be ascertained by considering Eq. (30) in the limit of large ρ so that the $J_1(K\rho)$ term can be replaced by its asymptotic form, but retaining only the positive exponential

$$b_s\to\sqrt{\frac{2}{\pi}}\frac{e^{-i\pi/4}}{2i\sqrt{\rho}}\int_0^\infty\frac{dK}{K^{3/2}}J_1(K)e^{i\phi(K,\rho,\xi)}, \tag{42}$$

where

$$\phi=K\rho+\frac{\xi}{[1+(K/s)^2]^{1/2}}, \tag{43}$$

and $K\rho\gg 1$.

Taking the first derivative of ϕ with respect to K results in the condition for stationary phase

$$\frac{\rho}{\xi}=\frac{K/s^2}{[1+(K/s)^2]^{3/2}}, \tag{44}$$

which has real roots (in K) for $\rho<\rho_c$. For $\rho<\rho_c$ there are two real roots which coalesce at ρ_c into the value $K_c=s/\sqrt{2}$. Since at $K=K_c$, $d\phi/dK=d^2\phi/dK^2=0$, the dominant contribution to the integral is obtained by expanding ϕ through the third derivative

$$b(\rho\sim\rho_c,\xi\gg 1)\to\sqrt{\frac{2}{\pi}}\left(\frac{1}{\sqrt{\rho}}\right)\frac{J_1(K_c)}{K_c^{3/2}}\frac{e^{-i\pi 4}}{2i} \otimes\exp\left[\frac{i2\xi}{(3/2)^{3/2}}\right]\int_0^\infty dK\ e^{iK\Delta\rho}e^{i\alpha(K-K_c)^3}, \tag{45}$$

where $\alpha s^3=8\xi/(3)^{7/2}$ and $\Delta\rho=\rho-\rho_c$. The integral in Eq. (45) can be further manipulated into the sum of a driven Airy pattern (i.e., the function Gi) and a remaining integral having a small contribution (but not worth writing out in detail). The argument of the Gi function is $\Delta\rho/\rho_A$ with the scale length of variation near the maximum angle given by

$$\rho_A=\frac{1}{s}\left[\frac{8\xi}{(3)^{5/2}}\right]^{1/3}. \tag{46}$$

In summary, in the radiation zone, $\xi\gg 1$, the radial pattern of a KAW generated by a source with short transverse scale exhibits four distinct regions. For $\rho<1$ the contribution is dominated by the large-K domain in the integrand and is given by the quantity b_s of Eq. (38). In the region $1<\rho\ll\rho_c$ the pattern consists of the beat of two different wavelengths and is represented by b_s+b_L, with b_L given by Eq. (34). The beat merges continuously into a pattern of increasing radial wavelength that takes the form of a driven Airy function in the neighborhood of the radius coresponding to the maximum angle ($\rho\approx\rho_c$). Finally, within a few characteristic widths, given by Eq. (46), the radial oscillations disappear and the pure $1/r$ asymptotic behavior of Eq. (33) is achieved.

IV. NUMERICAL RESULTS

The spatial patterns obtained by direct numerical integration of Eq. (29) using a very fine mesh that has been tested for its ability to resolve the phase-mixing features of

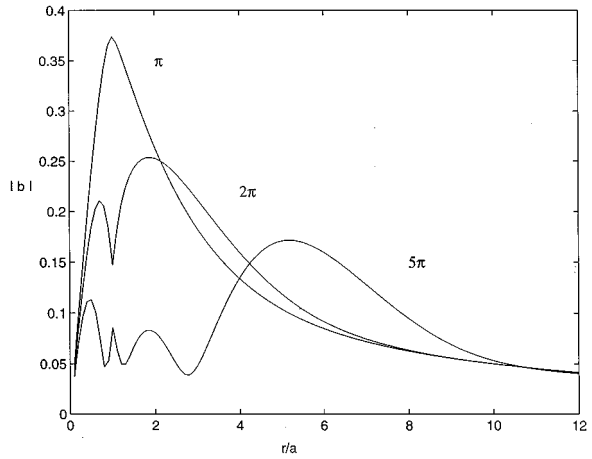

FIG. 1. Radial dependence of the magnitude of the scaled azimuthal magnetic field of a kinetic Alfvén wave at three different scaled axial positions $k_A z=(\pi,2\pi,5\pi)$ for a disk exciter whose radius equals ρ_s $(s=1)$ in the absence of collisions $(\Gamma_\parallel=0)$.

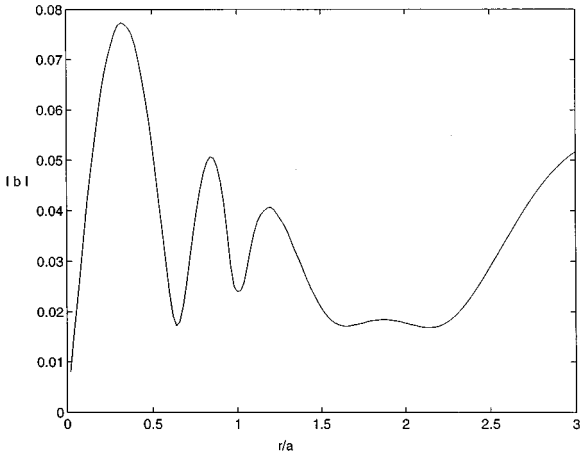

FIG. 3. Radial dependence in the vicinity of the disk exciter of the magnitude of the scaled azimuthal magnetic field at a large scaled axial position $k_A z=10\pi$ for $s=1$ and $\Gamma_\parallel=0$.

the integrand are examined in this section. First we concentrate on the patterns generated in the absence of collisions $(\Gamma_\parallel=0)$.

Figure 1 displays the magnitude of the scaled magnetic field for three different axial positions $(\pi\leqslant\xi\leqslant5\pi)$ for $s=1$. It is observed that at $\xi=\pi$ (near the current modulator) the azimuthal magnetic field increases nearly linearly for $r<a$ and falls off as $1/r$ for $r>a$, as is characteristic of a uniform current channel. At $\xi=2\pi$ the peak initially located at the edge of the exciter decreases sharply and a splitting of the pattern results. A short scale length oscillation develops for $r<a$ and a pattern of increasing radial wavelength spreads the current channel giving rise to a peak, near $r/a=5$ for $\xi=5\pi$, that eventually joins smoothly onto the $1/r$ asymptotic dependence. This behavior is to be compared to that of an Alfvén wave in the inertial regime which is shown in Fig. 2 for an equivalent small exciter (also having uniform current) having $a=c/\omega_{pe}$ (i.e., $p=1$). It is seen that in the inertial regime the propagation along cone trajectories causes the spreading pattern to join sharply (discontinuous derivative) onto the $1/r$ behavior. Also, the slope of the pattern for small r/a decreases rapidly as ξ increases. This implies that, on-axis, the current channel is depleted by coaxial induction currents generated by the skin effect. However, for the KAW the on-axis current remains well confined, as is seen in the slope of the curves in Fig. 1, and is a consequence of radially propagating signals that converge on the axis of symmetry.

The pinching of the on-axis current is illustrated by the pattern of the magnetic field seen in the region $r/a<1$ at large axial distances from the exciter, as shown in Fig. 3 for $\xi=10\pi$. The value of the slope of $|b|$ as $r\to0$ has been checked to agree with the prediction of Eq. (39) and the oscillations have also been found to follow the dependence expected from Eq. (38). It is seen from Fig. 3 that for $r/a>1$ the short scale oscillations evolve into a long scale pattern; this arises from the beat of the b_s and b_L terms. For larger values of r/a, however, this behavior makes a continuous transition to a pattern of increasing radial wavelength

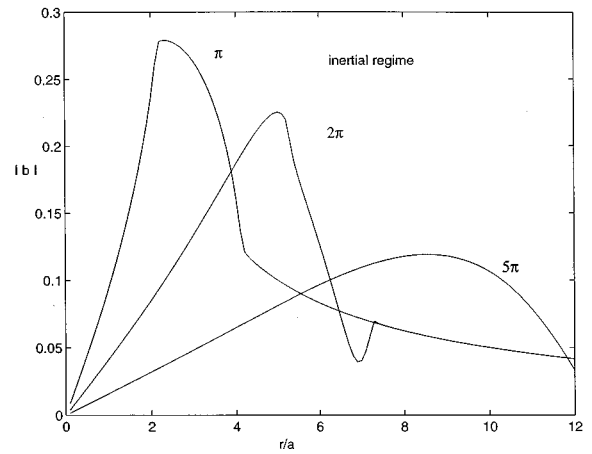

FIG. 2. Radial dependence of the magnitude of the scaled azimuthal magnetic field of an inertial Alfvén wave at three different scaled axial positions $k_A z=(\pi,2\pi,5\pi)$ for a disk exciter whose radius equals c/ω_{pe} (i.e., $p=1$ of Ref. 6) in the absence of collisions $(\Gamma_\parallel=0)$. To be compared to Fig. 1.

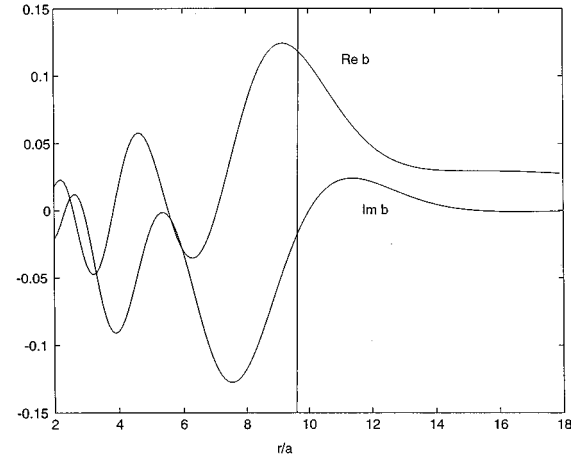

FIG. 4. Radial dependence of the real and imaginary parts of the scaled azimuthal magnetic field at a scaled axial position $k_A z=8\pi$ for $s=1$ and $\Gamma_\parallel=0$. The vertical solid line corresponds to the radial position associated with the maximum angle of propagation.

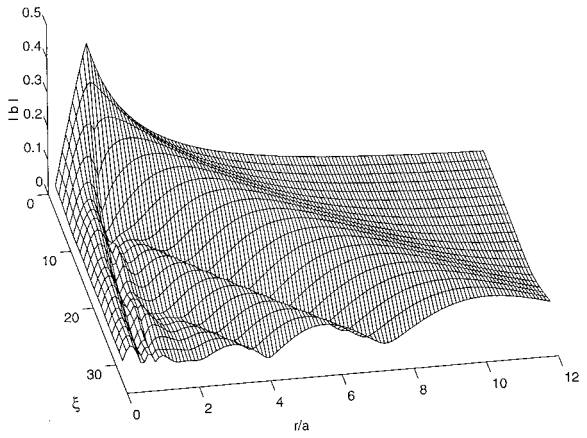

FIG. 5. Global perspective of the magnitude of the scaled azimuthal magnetic field illustrating the four different regions associated with the propagation of a KAW of short transverse scale. $s=1$ and $\Gamma_{\|}=0$.

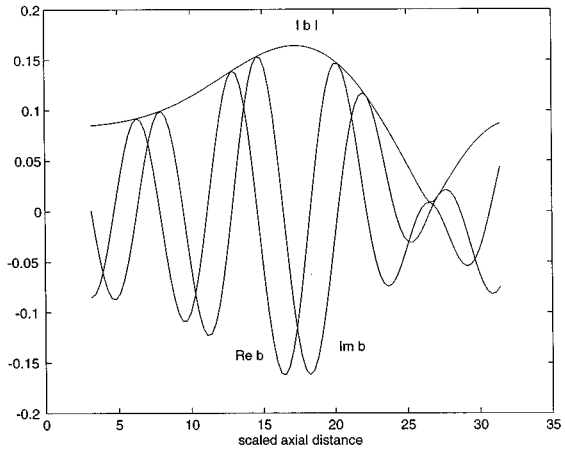

FIG. 7. Axial dependence of the scaled azimuthal magnetic field at a radial position $r/a=6$ for $s=1$ and $\Gamma_{\|}=0$. Parallel wavelength is close to $2\pi/k_A$. To be compared to Fig. 6.

analogous to that of a driven Airy function, as expected from Eq. (45) and clearly illustrated in Fig. 4 for $\xi=8\pi$. The solid vertical line in this figure corresponds to the value of the radial position ρ_c associated with the maximum angle of propagation. It is evident that radial wave propagation does not occur beyond ρ_c, only the $1/r$ asymptotic behavior exists in that region.

The characteristic four regions associated with the propagation of a KAW of short transverse scale are summarized in the more global, three-dimensional (3-D) display of Fig. 5.

As discussed in Sec. III, the parallel wavelength of a KAW changes from one field line to another in the absence of gradients in plasma parameters. This property is illustrated by Figs. 6 and 7 in which the axial dependence of the real and imaginary parts of the magnetic field are displayed. Figure 6 corresponds to a small radial position, $r/a=0.3$, and shows a relatively long parallel wavelength that increases with distance away from the exciter, as predicted by Eq. (40). The corresponding behavior at an intermediate radial position is illustrated in Fig. 7 for $r/a=6$. It is found that the parallel wavelength is much shorter than that of Fig. 6 and its numerical value is close to $2\pi/k_A$, as predicted by Eq. (34).

The changes produced by an increase in the electron temperature are illustrated in Fig. 8 at an axial location $\xi=3\pi$, still for $\Gamma_{\|}=0$. As the parameter s is decreased from 1 to 0.33 (i.e., T_e increases by a factor of 9 so that ρ_s is three times larger than the fixed radius of the exciter) the magnetic-field pattern remains well confined for $r/a<1$, but the behavior at large r/a exhibits a faster radial spread consistent with an increase in the maximum propagation angle with $(\beta_e)^{1/2}$ as described by Eq. (7). The global effect on the radiation pattern is illustrated in the 3-D display of Fig. 9 (for $s=0.33$), which is to be compared to Fig. 5.

The effects of increasing collisionality are illustrated in Fig. 10 for $s=1$ at an axial position $\xi=5\pi$. At a value of $\Gamma\equiv(\nu_e/\omega)(\delta/a)^2=0.25$ the short scale structure in the region $r/a<1$, associated with the axial pinching of the current channel, is smeared out but the peak corresponding to the maximum angle of propagation is still resolvable. However, for $\Gamma=1$ the intrinsic features of the KAW disappear and are

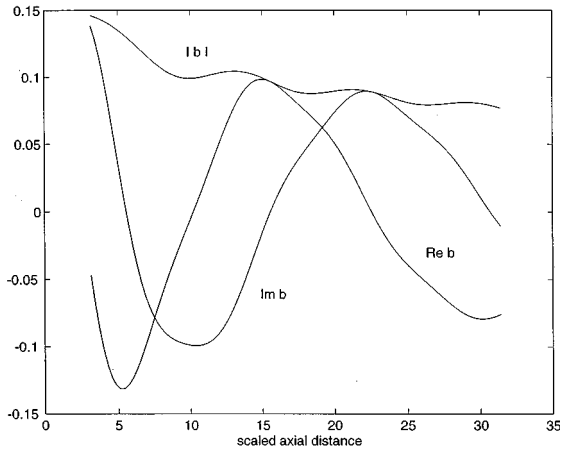

FIG. 6. Axial dependence of the scaled azimuthal magnetic field at a radial position close to the axis, $r/a=0.3$, for $s=1$ and $\Gamma_{\|}=0$.

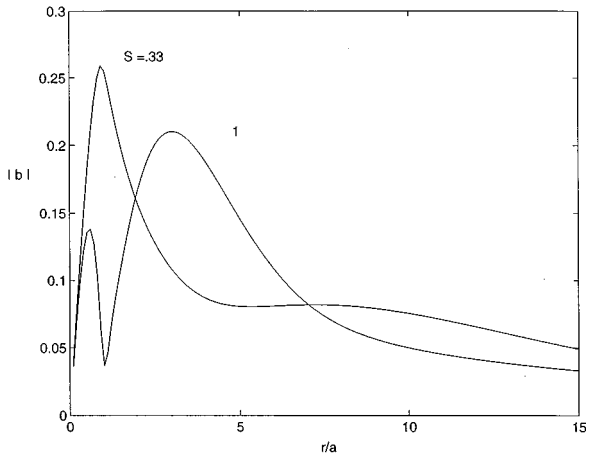

FIG. 8. Effect of increasing the electron temperature (decreasing s) on radial dependence of the magnitude of the scaled azimuthal magnetic field at a scaled axial position $k_A z=3\pi$ for $\Gamma_{\|}=0$. $s=a/\rho_s$.

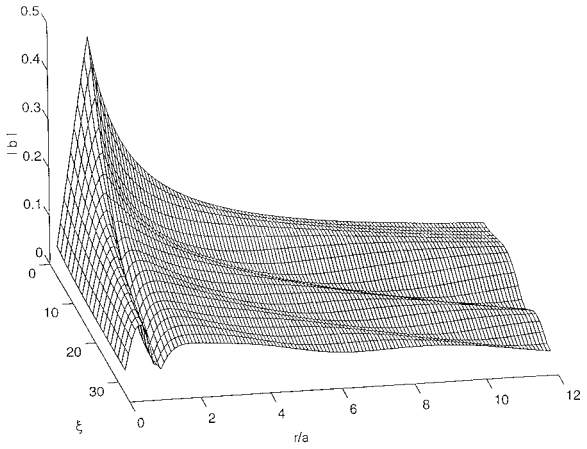

FIG. 9. Global perspective of the magnitude of the scaled azimuthal magnetic field for $s=0.33$, $\Gamma_{\|}=0$. To be compared to Fig. 5.

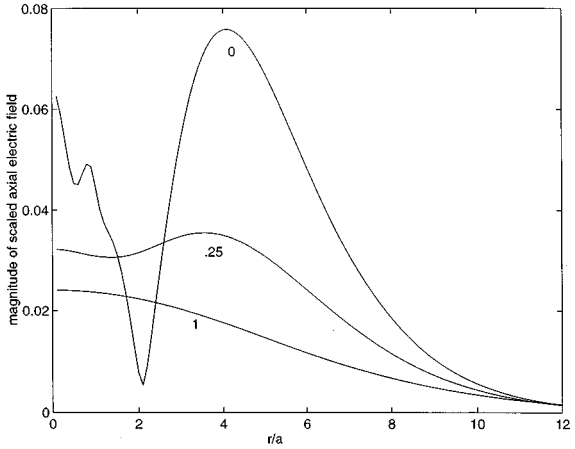

FIG. 11. Radial dependence of the magnitude of the scaled parallel electric field [given by Eq. (47)] associated with the magnetic-field patterns of Fig. 10.

replaced by a gentle diffusion pattern. This behavior is analogous to that exhibited by inertial Alfvén waves, as documented in Fig. 13 of Ref. 6.

The radial dependence of the magnitude of the scaled parallel electric field $|E_s|$ associated with the magnetic field patterns of Fig. 10 is displayed in Fig. 11, where

$$E_S=\frac{ia^2\omega_{pe}^2}{2\omega I_0[\beta_e(M/m)-i\Gamma_{\|}]}E_z$$
$$=\int_0^{\infty}dK\,\frac{J_1(K)J_0(K\rho)}{1+(K/s)^2}\,e^{iK_{\|}\xi}, \tag{47}$$

with $K_{\|}=k_{\|}(k)/k_A$ obtained from Eq. (18). It is seen from Fig. 11 that in the collisionless regime the electric field achieves its maximum value at a radial position well separated from the exciter (i.e., $r/a\approx 4$), but in the diffusive regime corresponding to large collisionality the electric field is essentially uniform across the exciter and fallsoff gently for $r/a>1$.

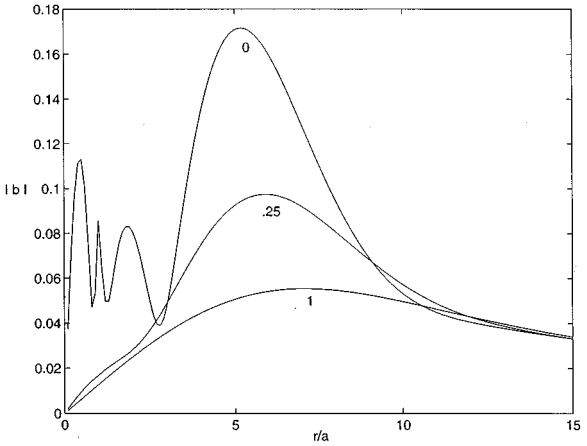

FIG. 10. Effect of increasing collisionality on the magnitude of the scaled azimuthal magnetic field at a scaled axial position $k_A z=5\pi$ for $s=1$. Collisional values correspond to $(\nu_e/\omega)(\delta/a)^2=0$, 0.25, and 1.

V. CONCLUSIONS

This analytical study has illustrated the intrinsic features of the spatial pattern exhibited by kinetic shear Alfvén waves excited by sources having small transverse scale length (on the order of c_s/Ω_i) in plasmas whose electron beta β_e is much larger than the electron to ion mass ratio, i.e., $\beta_e \gg m/M$. There are several areas of current research in which an understanding of these features may be of relevance, e.g., electron acceleration in the auroral ionosphere, the structure of filamentary current channels in astrophysical plasmas, and wave-mediated transport in magnetic confinement devices. In addition, some of the predicted features exhibit unique signatures (e.g., focusing on-axis [Eq. (39)], decreasing axial wavelength in a uniform medium [Eq. (40)]), which should be amenable to experimental investigation under controlled conditions in the laboratory. In particular the results obtained suggest that a systematic study of the pattern of shear Alfvén waves as the quantity β_e is varied is worth pursuing, especially if the region near the axis of the exciter can be probed.

The results obtained in this study indicate that under low collisionality conditions the patterns of shear Alfvén waves excited by small sources are fundamentally different in the inertial and kinetic regimes. The properties in both cases are controlled by unique propagation angles; in the inertial case the relevant angle is the cone angle given by $\tan\theta_c=(\omega/\Omega_i)\times(m/M)^{1/2}$ while in the kinetic regime the pattern spreads radially up to a maximum angle given by $\tan\theta_M=(\omega/\Omega_i)\times(\beta_e)^{1/2}/2.6$. The consequences of these two different physical propagation characteristics should be considered and contrasted when interpreting measurements of Alfvénic fluctuations made by spacecraft as well as in laboratory experiments.

ACKNOWLEDGMENTS

This work is sponsored by the Office of Naval Research.

[1] J. E. Borovsky, J. Geophys. Res. **98**, 6101 (1993).
[2] P. Louarn, J. E. Wahlund, T. Chust, H. de Feraudy, A. Roux, B. Holback, P. O. Dovner, A. I. Ericksson, and G. Holmgren, Geophys. Res. Lett. **21**, 1847 (1994).

[3]A. Strelsov and W. Lotko, J. Geophys. Res. **100**, 19,457 (1995).
[4]G. J. Morales and H. Ramachandran, *International Conference on Plasma Physics, Innsbruck, 1992* (European Physical Society, Petit-Lancy, 1992), Vol. 16C, p. I-135.
[5]T. Ohkawa, Phys. Lett. A **67**, 35 (1978).
[6]G. J. Morales, R. S. Loritsch, and J. E. Maggs, Phys. Plasmas **1**, 3765 (1994).
[7]G. G. Borg, M. H. Brennan, R. C. Cross, L. Giannoue, and I. J. Donnely, Plasma Phys. Controlled Fusion **27**, 1125 (1985).
[8]P. M. Bellan, Geophys. Res. Lett. **23**, 1717 (1996).
[9]W. Gekelman, D. Leneman, J. Maggs, and S. Vincena, Phys. Plasmas **1**, 3775 (1994).
[10]I. S. Gradshteyn and I. M. Ryzhik, *Tables of Integrals, Series and Products* (Academic, New York, 1965), p. 692, formula 6.575.
[11]*Tables of Integral Transforms*, edited by A. Erdélyi (McGraw-Hill, New York, 1954), Vol II, p. 47.
[12]This integral was first introduced by L. von Gegenbauer to evaluate the Weber–Schaftheitlen integral (which appears in the discussion of the inertial case). For details consult G. N. Watson, *Theory of Bessel Functions* (Cambridge University, Cambridge, England, 1944), p. 406.
[13]I. S. Gradshteyn and I. M. Ryzhik, *Tables of Integrals, Series and Products* (Academic, New York, 1965), p. 340, formula 11.